Int. J. Heat Mass Transfer. Vol. 37, No. 2, pp. 321–332, 1994
Printed in Great Britain

0017–9310/94 $6.00 + 0.00

High flux boiling in low flow rate, low pressure drop mini-channel and micro-channel heat sinks

M. B. BOWERS and I. MUDAWAR†
Boiling and Two-phase Flow Laboratory, School of Mechanical Engineering, Purdue University, West Lafayette, IN 47907, U.S.A.

(*Received* 20 *August* 1992 *and in final form* 11 *March* 1993)

Abstract—Due to the need for practical cooling technologies which could dissipate high heat fluxes, an experimental study of pressure drop and CHF in mini-channel ($D = 2.54$ mm) and micro-channel ($D = 510$ μm) heat sinks of 1 cm heated length was performed using R-113. Test conditions included inlet subcooling ranging from 10 to 32°C and a range of low flow rates up to a maximum of 95 ml min^{-1}. The tests yielded CHF values for both heat sinks in excess of 200 W cm^{-2} with the advantage of both low flow rates and low pressure drops ($\Delta P < 0.32$ bar) as compared to high-flux, single-phase micro-channel heat sinks. Key features of the miniature heat sinks include a lack of inlet subcooling effect on CHF and superheated outlet conditions at the lowest flow rates. A single CHF correlation was developed for both heat sinks. The paper will illustrate the use of the CHF correlation and a generalized model for pressure drop as predictive tools in assessing the merits of different channel sizes in incorporating miniature heat sink technology into high heat flux cooling schemes. Overall, the mini-channel's performance proved superior to the micro-channel due to pressure drops less than 0.01 bar for comparable CHF values as well as the reduced likelihood of clogging and the relative ease in fabricating the mini-channel.

1. INTRODUCTION

INCREASED demands for dissipating high heat fluxes from electronic, power, and laser devices creates the need for new cooling technologies as well as improvements in existing technologies. To meet such demands, miniature heat sinks of roughly one square centimeter in heated surface area are in the development stages. Such heat sinks consist of a thin block of metal that contains small channels for the flow of cooling fluid, which acts as a sink for heat supplied to the surface of the block. The heat sinks are typically characterized by channel hydraulic diameters ranging from roughly 90–550 μm [1, 2] and are referred to as micro-channels. The small hydraulic diameter insures a thin thermal boundary layer and results in a large heat transfer coefficient; however, the dissipation of high heat fluxes is accompanied by large pressure drops. Tuckerman and Pease [1] performed optimization studies for laminar flow of water through micro-channels of 1.0 cm^2 heated surface area. For a heat flux of 181 W cm^{-2} the corresponding pressure drop was 1.0 bar. In a separate study, Phillips [2] developed a computer code to predict both laminar and turbulent flow pressure drop and heat transfer characteristics for various liquids and micro-channel sizes. The reference case for water flow yielded heat fluxes of 100 W cm^{-2} and greater in a 1.0 cm long channel with a pressure drop of 0.69 bar.

In order to increase the heat flux from a micro-channel with single-phase cooling while maintaining practical limits on surface temperature, it is necessary to increase the heat transfer coefficient by either increasing the flow rate or further decreasing the hydraulic diameter. Both are accompanied by very large increases in pressure drop. However, two-phase heat dissipation can achieve very high heat fluxes for a constant flow rate while maintaining a relatively constant surface temperature, and the surface temperature's magnitude is generally determined by the saturation properties of the cooling fluid. The limiting factor for most convective boiling situations is the critical heat flux, CHF. When CHF is approached for a flow boiling system, there is a sudden dryout at the heat transfer surface which is accompanied by a drastic reduction in heat transfer coefficient and corresponding rise in surface temperature.

There are several advantages to utilizing two-phase miniature heat sinks over their single-phase counterparts. Key advantages are as follows:

(1) Single-phase miniature heat sinks compensate for high surface heat fluxes by a large stream-wise increase in coolant temperature and a corresponding stream-wise increase in the heat sink temperature. This increase is often very detrimental to temperature-sensitive devices such as electronic chips. Two-phase heat sinks, on the other hand, rely upon latent heat exchange which maintains stream-wise uniformity both in the coolant and the heat sink temperatures at a level set by the coolant saturation temperature.

† Author to whom all correspondence should be addressed.

NOMENCLATURE

A_f	heat sink total flow area normal to flow, $N(\pi D^2/4)$
c_p	specific heat
D	channel inside diameter
f_s	Fanning friction factor
f_{TP}	two-phase friction factor
G	mass velocity, $\rho_f Q_T/A_f$
h_{fg}	latent heat of vaporization
K	empirical constant
L	heated length of heat sink channel
L_b	boiling length of channel's heated section
L_o	outlet length of heat sink channel
L_s	length of channel's inlet single-phase region
L_{tot}	total length of channel
N	number of channels in heat sink
P	pressure
ΔP	pressure drop
q	heat flux based upon 1 cm^{-2} heated upper surface of heat sink
q_m	CHF based upon 1 cm^{-2} heated upper surface of heat sink
q_p	heat flux based upon the heated channel inside area, $q_m w/(N\pi D)$
$q_{m,p}$	CHF based upon the heated channel inside area
$q_{mo,p}$	CHF based upon channel inside area for condition of zero inlet subcooling
Q_T	total volumetric flow rate of heat sink
t	thickness of cell containing one channel
t_w	width of cross sectional cell containing one channel
T	temperature
T_s	reference surface temperature used in boiling curves
ΔT_{sub}	liquid subcooling, $T_{sat}-T$
U	mean liquid velocity at channel inlet
v	specific volume
v_{fg}	difference in specific volumes of saturated liquid and vapor
w	width of heat sink's heated upper surface, Nt_w
We	Weber number, $G^2L/(\sigma\rho_f)$
x	mass vapor quality
x_e	thermodynamic equilibrium quality
x_i	equilibrium quality at the channel inlet
x_L	equilibrium quality at the end of the heated length
z	coordinate in flow direction.

Greek symbols

ρ	density
σ	surface tension.

Subscripts

A	acceleration
exp	experimental data
f	liquid
F	friction
g	vapor
G	gravity
i	inlet
m	maximum (critical heat flux)
o	outlet
p	heat flux area based upon channel inside area
pred	analytical prediction
sat	saturated
sub	subcooled.

(2) In order to lessen the detrimental effects of stream-wise increases in coolant and heat sink temperatures, larger flow rates are often needed with single-phase micro-channel heat sinks. Two-phase heat sinks, on the other hand, permit the consumption of all liquid by evaporation, thus requiring minimal coolant flow rates.

An early study of CHF by Gambill and Greene [3] examined the flow of water through 7.74 mm i.d. vertical tubes of 4.70 cm length and greater. There was an increase in CHF values with increases in both exit subcooling and mean flow velocity, and a reduction in CHF with increased L/D. The CHF data was correlated in the form of Gunther's equation [4] which accounts for the effect of velocity and subcooling at $L/D = 6$; however, to increase the range of applicability, Gambill and Greene modified the correlation with a term which accounted for variations in L/D.

A generalized correlation of CHF for forced convection boiling in vertical tubes was later devised by Katto [5, 6]. Data for different liquids from various sources were separately analyzed and correlated for four distinct regimes called the L-, H-, N-, and HP-regimes. CHF for zero inlet subcooling, $q_{mo,p}$, was correlated as

$$\frac{q_{mo,p}}{Gh_{fg}} = f\left[\frac{\rho_f}{\rho_g}, \frac{\sigma\rho_f}{G^2L}, \frac{L}{D}\right]. \tag{1}$$

For most regimes, there was a linear rise in CHF with increased inlet subcooling; therefore, subcooling was accounted for by the following equation

$$q_{m,p} = q_{mo,p}\left[1 + K\frac{c_{p,f}\Delta T_{sub,i}}{h_{fg}}\right], \tag{2}$$

where K was empirically determined from the data base for each regime. Katto also concluded from his

study that, for the special case of a very long tube, CHF seemed to occur for the condition of exit quality equal to one.

The effect of inlet subcooling on CHF was later explored in a separate study by Katto [7]. In his revised correlation he utilized the boiling length, L_b, which is the heated length for a uniformly heated tube from the location where $x_e = 0$ to the end of the heated length or the location of $x_e = 1$ for the case of total dryout. The study defined a specific range where subcooled flow CHF can be found using the correlation described in equation (1) by replacing L with L_b.

Additional studies on CHF in vertical upflow have been performed using R-113 as the working fluid. Weede and Dhir [8] performed an experimental study for 1.73 cm i.d., uniformly heated tubes varying in L/D from 5.1 to 17.6. The data showed the common trends of increasing CHF with increasing inlet subcooling, decreasing L/D, and/or increasing mass velocity. Based upon the experimental trends, the data were correlated according to equations (1) and (2). Lazarek and Black [9] performed CHF studies with R-113 in a 12.6 cm long tube having an i.d. of 3.15 mm. They correlated their data in the form of a critical exit quality which was hypothesized as the trigger for the onset of CHF. The experimental values of critical quality covered a broad range with some as high as 89%.

Flow boiling can achieve high values of heat flux, but there are practical concerns in the design of high flux heat sinks other than CHF. A problem unique to flow boiling is the production of vapor bubbles that leads not only to increased heat transfer but also increased pressure drop. This is not unlike single phase flow in micro-channels where pressure losses are a problem; however, achieving high fluxes with flow boiling requires neither the relatively high flow rates for equal channel diameters of single-phase heat sinks nor the ultra small diameters that lead to very high pressure losses. The channel diameters required for comparable two-phase heat dissipation are on the order of 10–50 times larger than the micro-channels, thus referred to hereafter as mini-channels. An additional advantage of mini-channels is the ease of fabrication, whereas micro-channels require special manufacturing technology.

In this paper flow boiling in both mini-channel ($D = 2.54$ mm) and micro-channel ($D = 510\ \mu$m) heat sinks will be demonstrated as means of achieving high values of heat flux. The mini-channel diameter was chosen based upon manufacturing ease and tube flow CHF predictions. However, the micro-channel was selected from several provided by 3M and was specifically chosen for a practical comparison of boiling performance relative to the mini-channel. The flow boiling experiments were performed with R-113 at 1.38 bar to determine CHF for a range of inlet subcoolings and flow rates, and simultaneously, a data base was acquired for pressure drop as a function of both flow rate and heat flux. Based upon the experimental findings, a general description and comparison of the hydrodynamic and flow boiling characteristics of both the mini- and micro-channel heat sinks are presented. The experimental work is complemented by the development of a generalized pressure drop model for miniature heat sinks and a correlation for the CHF data base. Also included in this paper is a discussion on the use of the model and correlation as predictive tools for incorporating this technology into any high flux cooling scheme.

2. EXPERIMENTAL APPARATUS

In order to investigate mini- and micro-channel two-phase flow and heat transfer characteristics, the flow loop illustrated in Fig. 1(a) was constructed. R-113, the dielectric coolant chosen for this study, was pumped from the bottom of the loop reservoir and circulated through the loop by a magnetically coupled centrifugal pump. Exiting the pump, the liquid passed through a 5 μm cartridge filter followed by a heat exchanger where it was heated or cooled depending upon the test subcooling conditions. The appropriately metered volume flow rate then entered the test loop while the remaining flow was routed to the reservoir through a by-pass loop. The volume flow rate of R-113 that entered the test module was measured with a rotameter, and its magnitude was controlled by adjusting valves located in both the test loop and by-pass line.

A cartridge heater was used to fine tune the test loop's stream temperature, which was measured at both the inlet and exit of the test module with thermocouples located, respectively, in the tubing upstream and downstream of the test module. Exiting the module, the fluid flowed through a cooler to condense the large vapor fraction and then into the reservoir where the stream remixed with the by-passed liquid. To control the loop pressure, a liquid–vapor mixture was maintained in the pressure control tank, and loop pressure was adjusted by either heat addition or removal. Also connected to the pressure control tank was a reflux condenser which was used during dearcation of the fluid.

Test module

The test module in Fig. 1(b) was used for both heat sinks, and consisted of a housing and cover made from G-10 fiberglass plastic, which was chosen for both its insulating properties and dimensional stability. The mini- or micro-channel heat sink was fitted in the housing and held securely in place by the cover. The housing possessed both inlet and outlet plenums that were large enough to insure a uniform pressure in the plenum at the entrance to the heat sink and at the exit where the streams from the heat sink's flow channels remixed. This assured equal flow rates through the individual flow channels. Incorporated into the cover were pressure taps located at the inlet

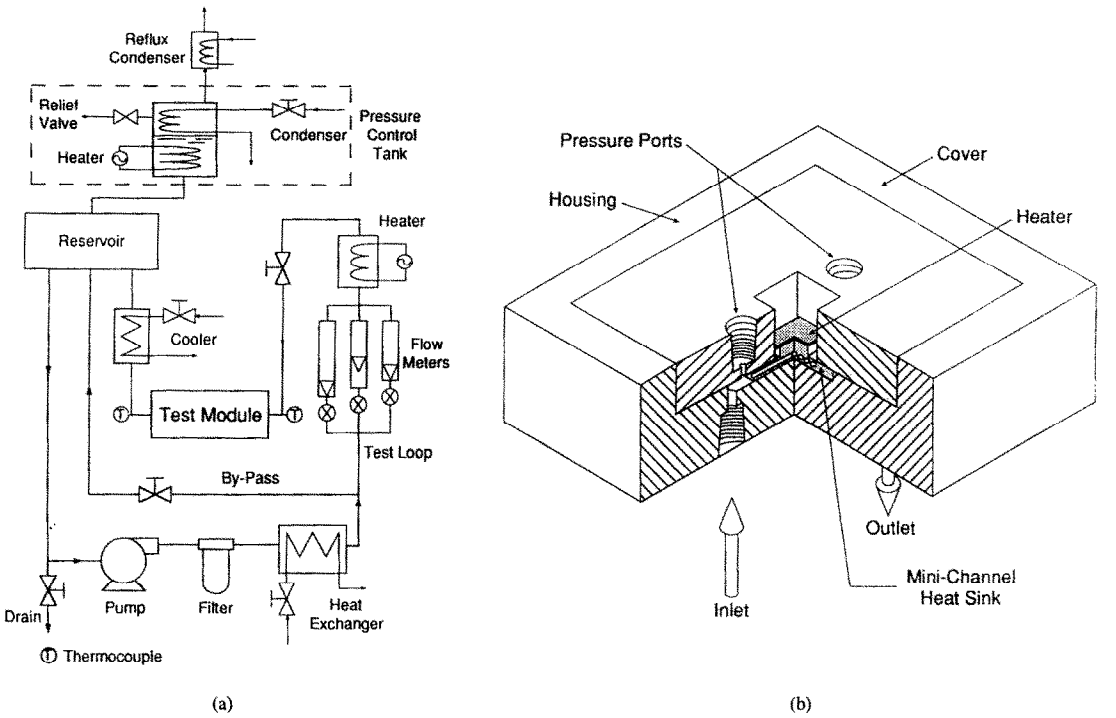

FIG. 1. (a) Flow loop and (b) test module.

and outlet plenums for measurement of both inlet pressure and pressure drop.

The miniature heat sinks are illustrated in Fig. 2. The mini-channel heat sink, Fig. 2(a), was machined from one block of oxygen-free copper. It consisted of a 10×10 mm^2 top section, to which a thick-film resistor was soldered, and a 28.6×28.6 mm^2 bottom plate through which the mini-channels were machined. The top section protruded 3.18 mm from the bottom plate and was designed to provide a uniform heat flux for a 1 cm^2 area. The thick-film resistor was powered by a 0–240 V a.c. variac. Directly below the top section and equidistant within a 1 cm width were three 2.54 mm i.d. channels that ran the entire length of the bottom plate, which had area larger than the heated top due to the necessity of providing mechanical seals. A 0.13 mm thermocouple for providing a reference temperature was located at the midpoint of the mini-channel's top section. The thermocouple was placed inside a 0.81 mm hole which was then filled with a thermally-conducting epoxy containing boron nitride.

The micro-channel heat sink, Fig. 2(b), was very similar to the mini-channel; however, it consisted of a separate nickel plate and a copper conducting block. The micro-channel plate, which contained 510 μm i.d. channels, required special manufacturing technology and was provided by 3M. The top section of the conducting block duplicated that of the mini-channel heat sink with the lower part serving as a spacer, and to provide a low thermal contact resistance between the conducting block and nickel plate, the two parts were silver-soldered together. To insure that channels within only a 1 cm width directly below the heat source were active, all channels except the middle 17 were filled with solder at both the channel inlets and outlets.

Data acquisition

Before performing experimental tests, the flow loop was prepared for operation which included periodic deareation of the fluid. This procedure was performed by vigorously boiling the R-113 to force the vapor and other entrained gases into the reflux condenser where the R-113 vapor condensed and drained back into the pressure control tank as the other non-condensable gases escaped freely to the ambient. Also on a periodic basis, the channels of the mini-channel heat sink were cleaned with cotton swabs and acetone, and the channels of the micro-channel heat sink were reamed with a small wire to preclude any buildup of deposits.

For normal testing procedure, the electrical power to the heater was adjusted by the variac to the desired level, and the heat sink was then allowed to reach steady conditions, which were achieved within minutes once the flow conditions were stabilized. However, due to the large vapor fractions produced within the nucleate regime, 15–20 min were often required to stabilize the flow loop conditions. Steady state was assumed when the standard deviation over a period of 30 s for 15 samples of the heat sink's thermocouple was less than 0.2°C; however, this con-

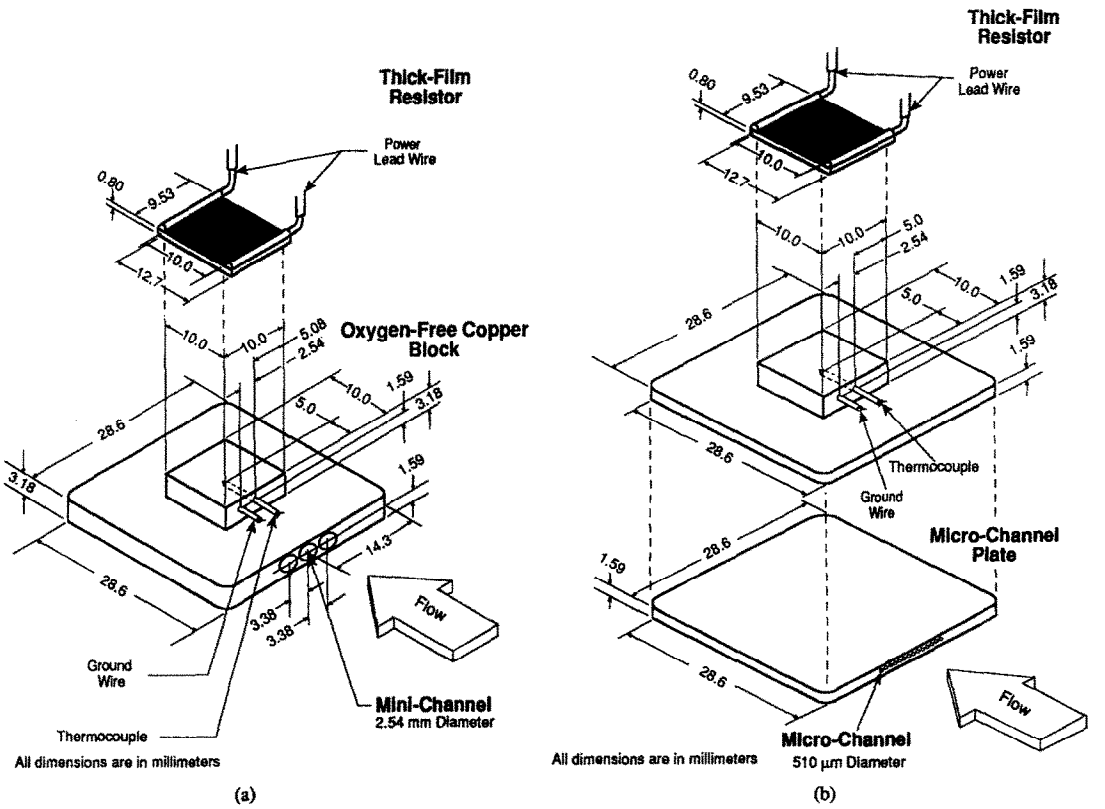

FIG. 2. (a) Mini-channel and (b) micro-channel heat sinks.

dition was relaxed for the very high fluxes (close to CHF) due to larger temperature fluctuations. At steady state, readings from all thermocouples, the watt meter, and both differential and absolute pressure transducers were recorded with a Keithley series 500 data acquisition system as directed by a Compaq microcomputer. Manual heat flux adjustments were done in increments of 10–20 W cm^{-2} in the nucleate regime, followed by 2 W cm^{-2} or less as CHF was approached. Boiling curves required 3–4 h and ended with CHF, which was identified by a sudden unbounded rise in the heat sink's temperature.

Measurement uncertainties

Errors associated with the thermocouples are estimated to be less than 0.2°C; however, due to the high heat fluxes, the heat sink thermocouple was facing large temperature gradients. The additional error associated with large temperature gradients was estimated to be less than 1.2°C at a heat flux of 200 W cm^{-2}. The uncertainty associated with differential pressure measurement was estimated to be less than 5% for the low pressures ($\Delta P < 0.02$ bar) and less than 1% for the higher differential pressures, and uncertainty in the absolute pressure was 1%. Error in flow rate measurement was estimated to be less than 4% with the greatest uncertainty being for the flow rates less than 34 ml min^{-1}.

Heat losses from the heat sink were numerically estimated to be less than 3%; therefore, electrical power measurement, which had an uncertainty of less than 1%, was used for heat flux calculations. The numerical predictions of heat loss were made assuming free convection boundaries for exposed surfaces and zero contact resistance between surfaces, thereby yielding conservative estimates of heat loss.

3. DISCUSSION OF RESULTS

Boiling data for flow of R-113 through both the mini-channel and micro-channel heat sinks were taken for a range of flow rate from 19 to 95 ml min^{-1} and inlet subcooling from 10 to 32°C while maintaining an inlet pressure of 1.38 bar. Tests were conducted to explore the effects of velocity and inlet subcooling on CHF as well as to compare the thermal and hydrodynamic performances of the two heat sinks.

Figure 3(a) compares the boiling curves of the mini- and micro-channel heat sinks for a flow rate of 64 ml min^{-1} and inlet subcooling of 20°C. For the single-phase portion of the curves, there is a distinct offset between the heat sinks' curves with the micro-channel exhibiting a lower thermal resistance. These results are to be expected since a small hydraulic diameter assures a thin thermal boundary layer, resulting in a larger heat transfer coefficient for the micro-channel. Also, the thermal resistance is further reduced by the larger number of channels in the micro-channel heat

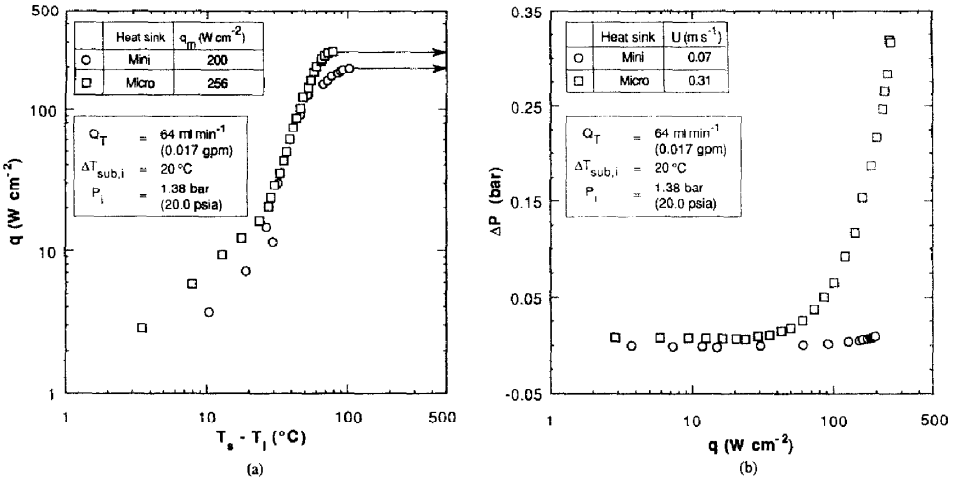

FIG. 3. Comparison of mini- and micro-channel (a) boiling curves and (b) pressure drops for a flow rate of 64 ml min^{-1} and 20°C inlet subcooling.

sink which results in a 14% increase in total circumferential area available for heat transfer. Figure 3(a) shows a slight hysteresis at incipience for the mini-channel; however, within the nucleate boiling regime, the distinction in thermal behavior subsides for all heat fluxes less than approximately 150 W cm^{-2}. Above this flux, the boiling curves diverge, with the mini-channel's curve displaying much more of the characteristic 'necking' before approaching CHF at 200 W cm^{-2} as compared to 256 W cm^{-2} for the micro-channel.

Pressure drop

For a flow rate of 64 ml min^{-1}, the micro-channel yielded a 28% increase in CHF as compared to the mini-channel; however, as illustrated in the corresponding pressure drop curves of Fig. 3(b), this required a substantial increase in pressure drop, from 0.008 bar for the mini-channel to 0.32 bar (3900% difference) for the micro-channel. Under single-phase conditions, the mini-channel pressure drops were negligible ($\Delta P < 0.003$ bar), as were the micro-channel's ($\Delta P \approx 0.007$ bar), due to the low flow rate employed. Once in the nucleate regime, the micro-channel pressure drops were observed to rise drastically with increased heat flux. A comparison of pressure drop in the nucleate boiling regime ($q = 100$ W cm^{-2}), where the thermal characteristics are indistinguishable, yields a $\Delta P \approx 0.003$ bar for the mini-channel and $\Delta P \approx 0.07$ bar for the micro-channel. These results clearly demonstrate a need for predictive tools for both the two-phase hydrodynamic and thermal behavior of mini- and micro-channel heat sinks. Such tools are of utmost importance in aiding the adaptation of miniature heat sink technology into any high flux application.

Subcooling effect

The effect of subcooling on the boiling characteristics is demonstrated in Fig. 4. Included on the figure are schematics of the heat sinks illustrating the reference temperatures, T_s, used in the presentation of the boiling curves and was calculated by assuming one-dimensional conduction from the plane of the thermocouple to the plane of T_s. The boiling curves are for a flow rate of 45 ml min^{-1} and inlet subcoolings of 10, 20, and 30°C. These plots illustrate a distinct offset between each subcooling in the nucleate boiling regime; however, this offset is simply a result of using inlet temperature in the temperature difference of the plot abscissa. The curves for each subcooling converge at high fluxes and yield the same values of CHF for each respective heat sink. As expected, the micro-channel yielded a larger CHF than the mini-channel's CHF. An explanation for this behavior is available from Fig. 5, which shows the outlet temperatures that correspond to the heat fluxes of Fig. 4. For heat fluxes below 20 W cm^{-2}, the outlet temperatures distinctively correspond to each value of inlet subcooling; however, for heat fluxes above 40 W cm^{-2}, the outlet temperature shows little dependence on inlet subcooling. The exit temperature corresponding to different subcoolings is indistinguishable for the higher heat fluxes because of the fluid being at saturated conditions. Therefore, the outlet temperature is the saturation temperature that corresponds to the exit pressure. The behavior described was characteristic of both heat sinks; however, the micro-channel, unlike the mini-channel, experienced a decrease in outlet temperature with increasing heat flux. Figures 6(a) and (b) demonstrate that this phenomenon is a result of the large rise in pressure drop in the micro-channel with increasing heat flux. The plots show the variation in outlet saturation temperature as a result of the decrease in outlet pressure as predicted by the model presented in the next section. In each case, the outlet subcooling reduces to zero for relatively very low values of heat flux; therefore, for the low flow rates considered in this study, there was a negligible effect of inlet subcooling on CHF.

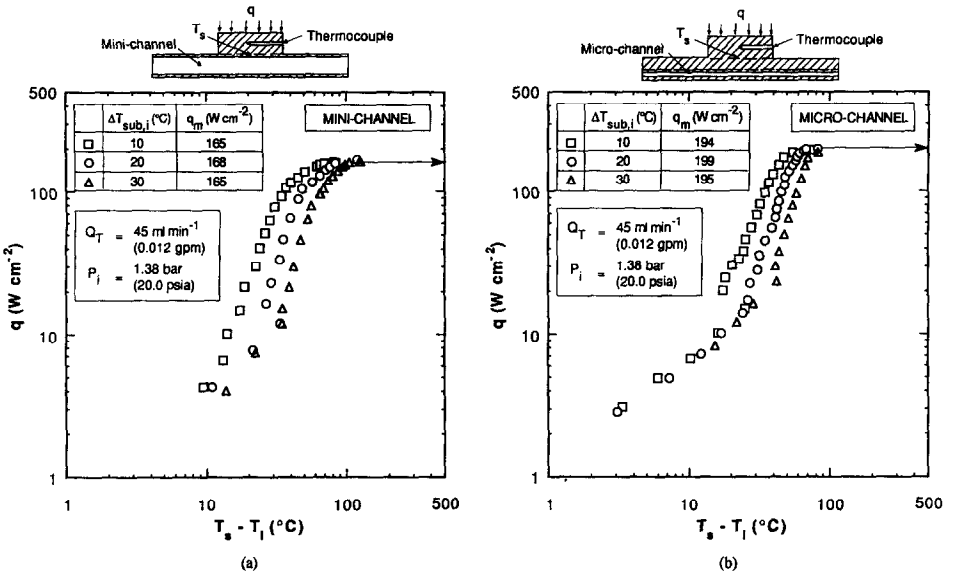

FIG. 4. Comparison of boiling curves for the (a) mini- and (b) micro-channel heat sinks for inlet subcoolings of 10, 20 and 30°C at a flow rate of 45 ml min^{-1}.

Superheated exit conditions

For test cases at the lowest flow rates ($Q_T < 19$ ml min^{-1}), the flow not only reached saturation conditions and possibly total dryout, but also superheated conditions as illustrated in Fig. 7. The plot is for the micro-channel at a flow rate of 19 ml min^{-1} and inlet subcooling of 20°C. The exit temperature is shown exceeding the outlet saturation temperature and assuming superheated values for heat fluxes even smaller than CHF. Superheated conditions at the outlet were observed not only for the micro-channel, but also for the mini-channel; however, superheated exit temperatures were encountered at lower flow rates with the mini-channel heat sink. These results suggest CHF is not always triggered by total dryout at the exit. This issue will be discussed in a later section.

4. PRESSURE DROP

To aid in the design of mini- and micro-channel heat sinks, a hydrodynamic model for predicting pressure drop was developed. With reference to Fig. 8, the heat sink is modeled as having N circular channels of diameter D, and each channel is contained within a rectangular cell with sides of lengths t and t_w.

Two-phase pressure drop

Evaluation of the pressure drop through a channel is based upon the homogeneous two-phase flow model. The model accounts for the total pressure gradient as the sum of contributions from friction, acceleration, and gravity, where the gravitational component is negligible for the heat sinks considered.

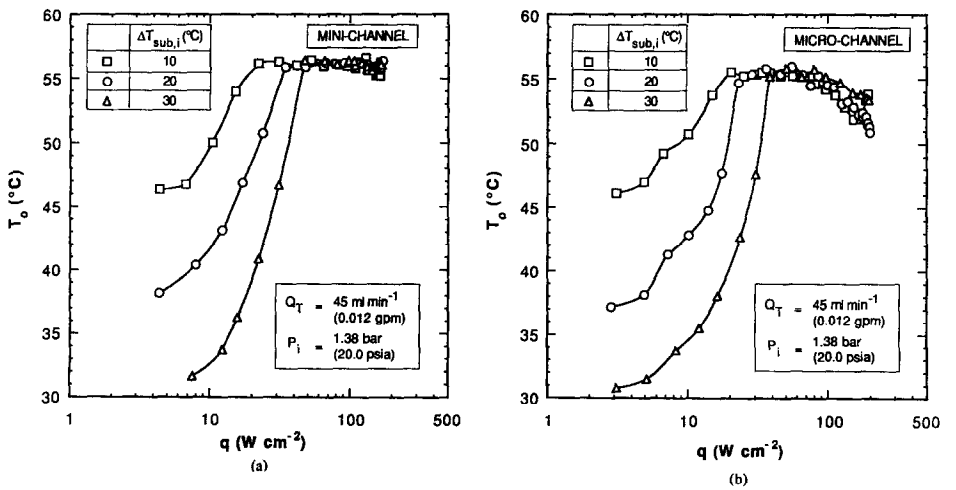

FIG. 5. Comparison of (a) mini- and (b) micro-channel outlet temperatures for inlet subcoolings of 10, 20, and 30°C at a flow rate of 45 ml min^{-1}.

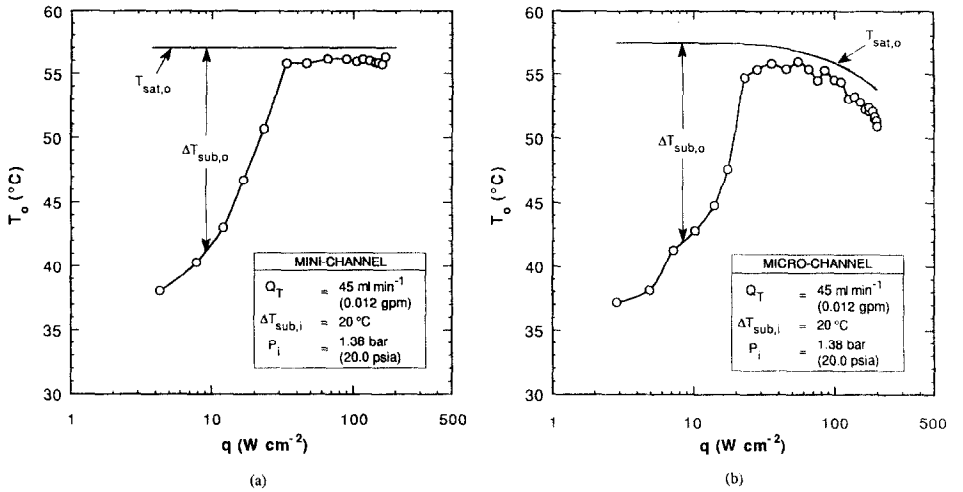

FIG. 6. Measured exit fluid temperatures and predicted exit saturation temperatures for (a) mini-channel with negligible pressure drop and (b) micro-channel with large pressure drop.

For the purposes of the present analysis, all properties are assumed constant. This assumption yields [10]

$$-\left(\frac{dP}{dz}\right)_F = \left(\frac{2 f_{TP} G^2}{\rho_f D}\right)\left[1.0 + x\left(\frac{v_{fg}}{v_f}\right)\right], \quad (3a)$$

and

$$-\left(\frac{dP}{dz}\right)_A = \left(\frac{G^2}{\rho_f}\right)\left(\frac{v_{fg}}{v_f}\right)\frac{dx}{dz}. \quad (3b)$$

The flow quality, x, is assumed equal to the equilibrium quality, x_e, for $0 < x_e < 1$. The equilibrium quality is determined by employing conservation of energy on a differential control volume along the channel. The resulting differential expression for the equilibrium quality is

$$\frac{dx_e}{dz} = \frac{1}{h_{fg}}\left(\frac{N}{\rho_f Q_T}\right) q_p \pi D. \quad (4)$$

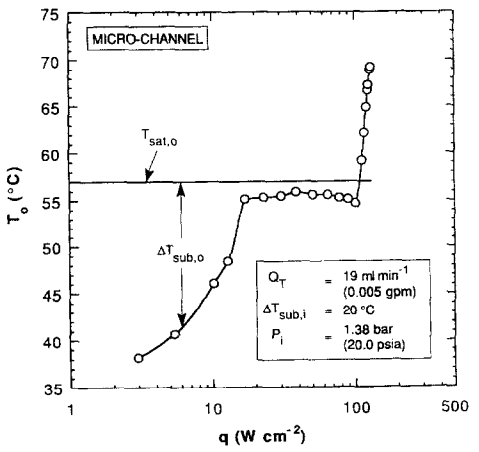

FIG. 7. Superheated exit conditions for flow rate of 19 ml min^{-1} as illustrated with measured exit fluid temperatures and predicted exit saturation temperatures.

Integrating the enthalpy gradient in equation (4) with the assumptions of constant heat flux and constant properties yields

$$x_e = \left(\frac{N q_p \pi D}{\rho_f Q_T h_{fg}}\right) z + x_i. \quad (5)$$

Substituting equations (5) and (4) in equations (3a) and (3b), respectively, the frictional and accelerational pressure drops are found by integrating over the chan-

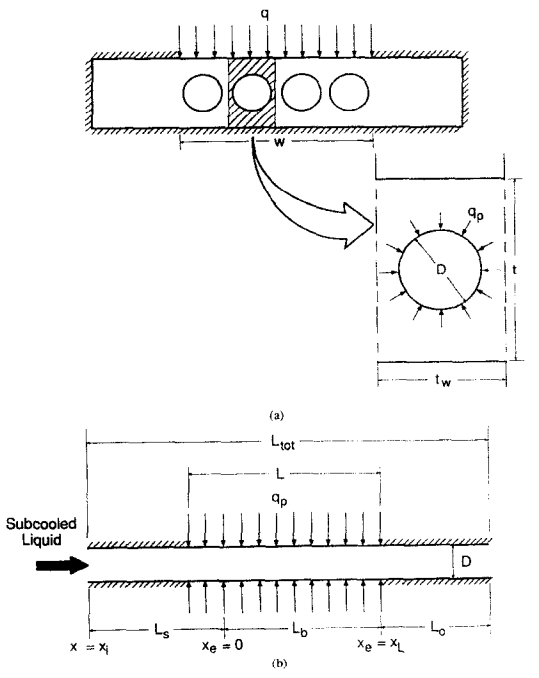

FIG. 8. Schematics illustrating mini- or micro-channel heat sink geometry with uniform heat flux, q, applied along the upper surface. Cross section in (a) defines the mean heat flux, q_p, around the channel inside area. The channel side view (b) defines the model nomenclature for a subcooled inlet.

nel's boiling length, L_b. Rewriting in terms of x_L, the equilibrium quality at the end of the heated length, yields

$$\Delta P_F = \left(\frac{2 f_{TP} G^2 L_b}{\rho_f D}\right)\left[1+\left(\frac{x_L}{2}\right)\left(\frac{v_{fg}}{v_f}\right)\right], \quad (6a)$$

and

$$\Delta P_A = \left(\frac{G^2}{\rho_f}\right)\left(\frac{v_{fg}}{v_f}\right)(x_L). \quad (6b)$$

The total pressure drop in the boiling region ($0 < x_e < 1$) is the sum of the contributions of acceleration and friction.

$$\Delta P_b = \Delta P_F + \Delta P_A. \quad (7)$$

The mass velocity, G, can be defined in terms of the total flow rate and flow area which is then substituted into equations (6a) and (6b). Regrouping yields

$$\left[\frac{\Delta P_F}{\left(\frac{16\rho_f}{\pi^2 L_b^2}\right)\left(\frac{Q_T}{w}\right)^2}\right]\left(\frac{D}{t_w}\right)^2 = 2 f_{TP}\left[1+\left(\frac{x_L}{2}\right)\left(\frac{v_{fg}}{v_f}\right)\right]\left(\frac{L_b}{D}\right)^3, \quad (8a)$$

and

$$\left[\frac{\Delta P_A}{\left(\frac{16\rho_f}{\pi^2 L_b^2}\right)\left(\frac{Q_T}{w}\right)^2}\right]\left(\frac{D}{t_w}\right)^2 = x_L\left(\frac{v_{fg}}{v_f}\right)\left(\frac{L_b}{D}\right)^2, \quad (8b)$$

which are dimensionless relations for the frictional and accelerational pressure drops.

Comparison with experimental data

In order to accurately determine the total pressure drop for the mini- or micro-channel heat sinks, the pressure drop from the entrance and exit lengths must be included as well as the heated length upstream of the point where $x_e = 0$. To account for each contribution, the total pressure drop is written as

$$\Delta P = \Delta P_s + \Delta P_b + \Delta P_o, \quad (9)$$

where the respective subscripts refer to single-phase, boiling, and outlet sections of the channel. The single-phase length of the channel, L_s, is the sum of the unheated entrance and the heated section up to the location of $x_e = 0$ (see Fig. 8(b)) which can be determined from equation (8).

The single-phase pressure drop is given by

$$\Delta P_s = \frac{2 f_s G^2 L_s}{\rho_f D}, \quad (10)$$

where f_s is the Fanning friction factor whose value is determined from the Reynolds number for each of the unheated lengths as found in ref. [11]. The remaining portion of the heated length is the boiling length, L_b, for which $0 < x_e < 1$. The two-phase pressure drop relationships derived for frictional and accelerational pressure drop are valid within the convective boiling region; thus, equations (6a), (6b), and (7) are used to calculate the pressure drop for the remaining heated section assuming no superheating takes place within the heated section.

Over the length L_o, which extends from the end of the heated section through the channel outlet, the quality remains constant at a value equal to x_L. The two-phase frictional pressure drop is found by integrating equation (3a) for the exit length of the channel. This yields

$$\Delta P_o = \left(\frac{2 f_{TP} G^2 L_o}{\rho_f D}\right)\left[1+x_L\left(\frac{v_{fg}}{v_f}\right)\right], \quad (11)$$

which is also the total pressure drop in the exit length in the absence of any acceleration.

Pressure drop predictions based on equation (9) are compared with experimental data in Fig. 9. For the two-phase friction factor, Collier [10] gives a range from 0.0029 to 0.005; therefore, a conservative value of $f_{TP} = 0.005$ was used. Excluded from the data shown are those for which $x_e > 1$ at the end of the heated section. Also, calculations of the two-phase Mach numbers yielded a maximum value of 0.46 with 90% of the data having Mach numbers less than 0.28. Therefore, the assumption of constant properties is justified due to the small compressibility effects. The experimental pressure drop data are for mean values of 15 samples over a period of 30 s. The use of mean values is due to pressure drop fluctuations during testing. The standard deviations of these fluctuations for the micro-channel were generally around 2% up to a high of 8% at the lower values of pressure drop. The mini-channel yielded the greatest percentage fluctuation with standard deviations as high as 30% for

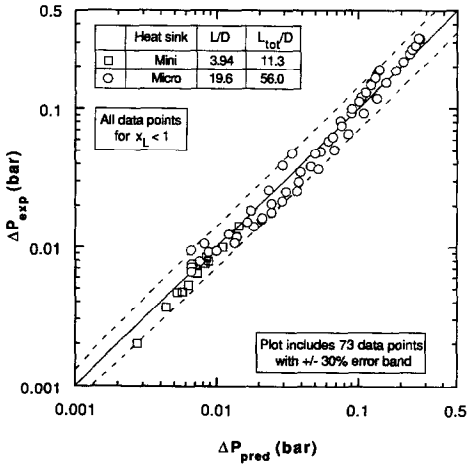

FIG. 9. Comparison of theoretical predictions of pressure drop with experimental data.

$\Delta P < 0.01$ bar due, in part, to the limited resolution of the differential pressure transducer for these very low pressures. The plot includes 73 data points; however, most are for the micro-channel because of its broader range of pressure drops. The model closely predicts the pressure drops as illustrated by the $\pm 30\%$ error band with the best predictions being for pressure drops exceeding 0.06 bar. Heat sink inlet and outlet pressure losses between the channel and the plenums are not included in the model; however, calculations show that the net contribution from both the acceleration or deceleration and form pressure drops is less than 0.7% of the total pressure drop. Based upon the model, the major contributor to the total pressure drop was determined to be the two-phase accelerational component calculated from equation (6b). For the micro-channel, the acceleration accounted for approximately 75% of the total pressure drop, compared to approximately 90% for the mini-channel. These results are to be expected due to the low mass velocities yielding low frictional losses. For the high flow qualities produced, a departure from the homogeneous assumption of dispersed flow to an annular flow would be expected; however, with the large liquid to vapor density ratio, evaporation is accompanied by a large acceleration in the flow that is accounted for in the model.

5. CHF CORRELATION

The CHF data base exhibited a lack of subcooling effect on CHF for both heat sinks and all operating conditions. The effect of mass velocity on CHF is illustrated in Fig. 10(a). The data base covers a mass velocity range from 31 to 150 kg m^{-2} s^{-1} for the mini-channel and 120 to 480 kg m^{-2} s^{-1} for the micro-channel. The data points follow a well defined trend with mass velocity with a high degree of repeatability. There is a distinct separation between the mini- and micro-channel curves as is expected due to the large difference in heated length-to-diameter ratio, 3.94 for the mini-channel compared to 19.6 for the micro-channel.

Due to a lack of CHF correlations for boiling in micro-channels, the CHF dependence on mass velocity for each heated length-to-diameter ratio was used to correlate the data. Since CHF is not sensitive to inlet subcooling, the standard CHF correlation form presented in equation (1) was used and resulted in the following correlation:

$$\frac{q_{m,p}}{Gh_{fg}} = 0.16\, We^{-0.19}\left(\frac{L}{D}\right)^{-0.54}. \qquad (12)$$

as shown in Fig. 10(b), where $q_{m,p}$ is CHF based upon the heated channel inside area. Heat flow predictions made using a finite element code with a constant surface heat flux and constant channel wall temperature revealed that 99% of the heat passes through the upper half of the channel for both the mini- and micro-channel heat sinks. Therefore, the channel inside area was used in the correlation to represent an average heat flux. Also included in Fig. 10(b) is the equilibrium quality that corresponds to each CHF value, and designated on the plot are values of CHF where superheated exit conditions similar to those shown in Fig. 7 were measured. For the mini-channel, only data for the lowest flow rates produced $x_L > 1$, whereas the micro-channel exhibited $x_L > 1$ for all data except the highest flow rate. This is expected since the micro-channel achieved higher CHF values than the mini-channel at all values of flow rate.

These CHF results point to unique features of miniature channel heat sinks not available in most other boiling systems. Of special importance to high flux cooling applications are the following features:

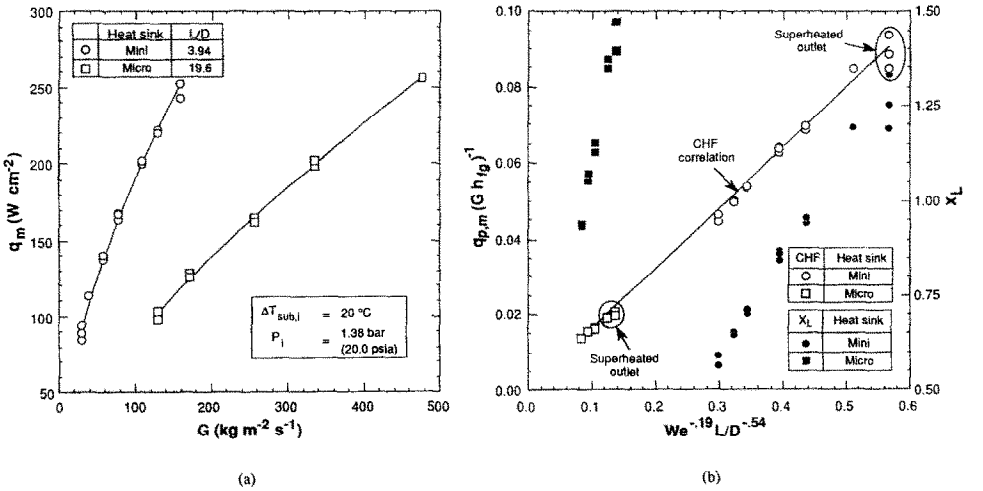

(a) (b)

FIG. 10. (a) Effect of mass velocity on CHF for mini-channel and micro-channel heat sinks and (b) the resulting correlation of CHF data and corresponding values of outlet equilibrium mass vapor quality for $\Delta T_{sub,i} = 20°C$.

(1) The two heat sinks demanded minimal flow rates evidenced by the values of x_L approaching or exceeding unity.

(2) The small diameters of the mini- and micro-channels suggest an increased frequency and effectiveness of droplet impact with the channel wall in regions of high x_L values. This may have greatly increased the heat transfer coefficient in that region, and enhanced CHF, compared to droplet flow regions in large diameter tubes.

(3) The small overall size of the heat sink seems to greatly contribute to delaying CHF by conducting heat away from the downstream region undergoing either partial or total dryout to the boiling region of the channel. No other system known to the authors has produced values of x_L exceeding unity at CHF.

6. DESIGN CONSIDERATIONS

Practical design tools have been established in the form of a CHF correlation and pressure drop model applicable to the mini- and micro-channel heat sinks of this study as well as miniature heat sinks of varying sizes. Figure 11 presents curves that characterize both CHF and the corresponding pressure drop for the mini- and micro-channel heat sinks at conditions for which $x_L < 1$. The CHF curves were constructed using the correlation of equation (12), and the pressure drop curves were constructed from equations (6) and (7). For illustrative purposes, a maximum heat flux requirement (i.e. CHF) of 500 W cm^{-2} based on the 1 cm^2 heater surface area has been assigned. To achieve 500 W cm^{-2} with the mini-channel necessitates a flow rate of approximately 270 ml min^{-1} as compared to a flow rate of roughly 200 ml min^{-1} for the micro-channel. Both flow rates are low considering the high heat flux required. However, the slight advantage of a lower flow rate with the micro-channel heat sink is recognized with a very high penalty in pressure drop,

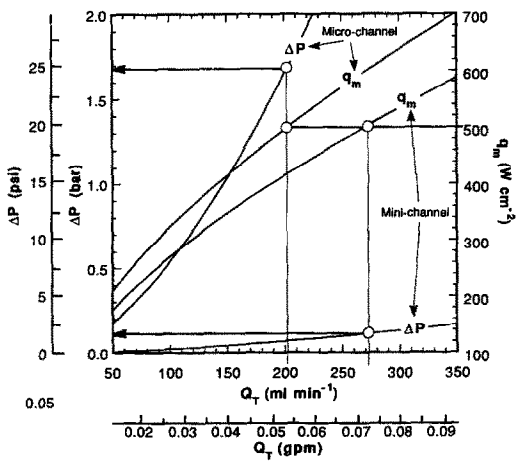

FIG. 11. Design plot illustrating flow rate and pressure drop characteristics to achieve a CHF of 500 W cm^{-2} with mini-channel and micro-channel heat sinks with $x_L < 1$.

1.7 bar compared to only 0.1 bar for the mini-channel heat sink. As demonstrated by the plot for this particular example, the mini-channel clearly possesses superior overall performance. Furthermore, mini-channels are much less likely to promote flow clogging than micro-channels. However, as evident by the diverging CHF curves, higher heat flux values may necessitate the use of the micro-channel, if the high pressure drop can be tolerated, or a heat sink with channel diameters between those considered in the present example due to constraints such as maximum flow rate.

By generating plots similar to those of Fig. 11 for a variety of heat sink channel sizes, a good comparison of performance characteristics can be obtained. Plots of this type do not yield a single optimum heat sink size; however, optimization schemes do not account for important practical concerns. Cooling schemes are generally limited by flow rate and pressure drop constraints as well as issues such as ease of fabrication and maintenance of the device. The above constraints are unique to each cooling scheme and must be carefully evaluated by the designer. Thus, the findings of this study provide information that is imperative to a designer incorporating mini- or micro-channel heat sinks into a high flux cooling scheme.

7. CONCLUSIONS

An experimental study of CHF in mini-channel ($D = 2.54$ mm) and micro-channel ($D = 510$ μm) heat sinks of 1 cm in heated length was conducted. Tests were performed for a range of inlet subcooling and flow rate. Complementing the experimental work are a pressure drop model and CHF correlation which provide analytical tools for heat sink design. Key findings of the study are as follows:

1. Flow boiling in mini- and micro-channel heat sinks is an effective means of achieving high heat fluxes ($q > 200$ W cm^{-2}) coupled with low flow rates ($Q_T < 65$ ml min^{-1}) and low pressure drops ($\Delta P < 0.35$ bar). In comparison, single-phase micro-channel technology reported in ref. [1] required a pressure drop of 1 bar to achieve a heat flux of 181 W cm^{-2} using water which has far superior thermal properties than the dielectric liquid utilized in the present study.

2. Reference [3] hypothesized that CHF was triggered by critical exit qualities; qualities as high as 89% were reported in that study with R-113 in 3.15 mm i.d. tubes of 12.6 cm heated length. Reference [6] also reported that CHF in long tubes appeared to occur at an exit quality approaching unity. However, the present study employed heat sinks which relied upon heat exchange with an array of small diameter channels with short heated lengths that were formed in a thermally-conducting metallic block. This allowed the spread of heat to surface locations where it could be dissipated rather than creating a large

rise in surface temperature. The net result was total dryout, and, at the lowest flow rates, superheated exit conditions before CHF, which suggests CHF was triggered at a location upstream of the exit. This is evidence that, unlike most other boiling systems, cooling with miniature heat sinks is possible with an evaporation efficiency of unity (i.e. minimal coolant flow rate).

3. CHF for mini-channel and micro-channel heat sinks is not a function of inlet subcooling at low flow rates due to the fluid reaching the saturation temperature a short distance into the heated section of the channel.

4. The homogeneous equilibrium model accurately predicts the pressure drop for flow boiling in miniature heat sinks at low flow rates. The major component of pressure drop was the acceleration which accounted for roughly 90 and 75% of the mini-channel and micro-channel pressure losses, respectively.

5. The flow boiling performances of both the mini- and micro-channel heat sinks are superior to comparable single-phase technology; however, the mini-channel clearly has the practical advantage over the micro-channel. Mini-channel CHF values as high as 200 W cm^{-2} were achieved with a negligible pressure drop of less than 0.01 bar compared to 0.23 bar for the micro-channel. Furthermore, the mini-channel heat sink could be fabricated using conventional drilling while fabrication of micro-channel heat sinks requires special manufacturing technology and is more prone to flow clogging.

REFERENCES

1. D. B. Tuckerman and R. F. W. Pease, High-performance heat sinking for VLSI, *IEEE Electron Device Lett.* **EDL-2,** 126–129 (1981).
2. R. J. Phillips, Forced-convection, liquid-cooled micro-channel heat sinks, M. S. Thesis, Department of Mechanical Engineering, Massachusetts Institute of Technology, Massachusetts (1987).
3. W. R. Gambill and N. D. Greene, Boiling burnout with water in vortex flow, *Chem. Engng Prog.* **54,** 68–76 (1958).
4. F. C. Gunther, Photographic study of surface-boiling heat transfer to water with forced convection, *Trans. ASME* **73**(2), 115–123 (1951).
5. Y. Katto, A generalized correlation of critical heat flux for the forced convection boiling in vertical uniformly heated round tubes, *Int. J. Heat Mass Transfer* **21,** 1527–1542 (1978).
6. Y. Katto, A generalized correlation of critical heat flux for the forced convection boiling in vertical uniformly heated round tubes—a supplementary report, *Int. J. Heat Mass Transfer* **22,** 783–794 (1979).
7. Y. Katto, An analysis of the effect of inlet subcooling on critical heat flux of forced convection boiling in vertical uniformly heated tubes, *Int. J. Heat Mass Transfer* **22,** 1567–1575 (1979).
8. J. Weede and V. K. Dhir, Experimental study of the enhancement of critical heat flux using tangential flow injection. In *Fundamentals of Heat Transfer in Fusion Systems* ASME HTD-24, pp. 11–18 (1983).
9. G. M. Lazarek and S. H. Black, Evaporative heat transfer, pressure drop and critical heat flux in a small vertical tube with R-113, *Int. J. Heat Mass Transfer* **25,** 945–960 (1982).
10. J. G. Collier, *Convective Boiling and Condensation* (2nd Edn). McGraw-Hill, London (1981).
11. R. W. Fox and A. T. McDonald, *Introduction to Fluid Mechanics* (3rd Edn) Wiley, New York (1985).